DESIGN CONSIDERATIONS FOR A SPACE-BORNE OCEAN SURFACE LASER ALTIMETER

Henry H. Plotkin
NASA Goddard Space Flight Center

Introduction

The desirable features of pulsed lasers as components of a satellite tracking system were recognized very soon after their initial development (Fig. 1). After design of some tentative systems, NASA launched the Beacon-Explorer B in 1964, containing fuzed silica retroreflectors especially for laser tracking. Several stations were soon ranging successfully, with precision generally about 2 meters. Other satellites were soon launched, so that there are now seven earth-orbiting arrays of laser retroreflectors (Fig. 2). The four arrays on the lunar surface are also used for the same purpose.

Precision and accuracy of present laser ranging systems are in the neighborhood of 25 cm. The systems now being built with state-of-the-art components are expected to achieve 10 cm or even better. Such techniques, applied to earth satellites have great value in geodesy and earth physics studies. Our task here is to examine how we might turn the system around: with the ranging system in the spacecraft, to reflect pulses vertically from the ocean surface, and so measure spacecraft altitude with great precision. For each such measurement, we assume the spacecraft position is known well enough so that the result will be a precise map of the shape of the ocean surface. This could be studied under varying tidal, seasonal, ocean current, and wind conditions.

Many of the features of a laser satellite ranging system are similar to those of an ocean surface altimeter. On the other hand, the altimeter also presents new problems. Some preliminary designs have already been suggested (see Ref. 1, 2, 3). A laser altimeter with considerably less sensitivity and resolution than we require was successfully flown on Apollo 15 to provide metric information for lunar photographs (Ref. 4) (Fig. 3) (Appendix A).

DESIRABLE FEATURES OF PULSED LASERS FOR SATELLITE TRACKING

- Very short pulses

- High power

- Good collimation with small antennas

- S/C reflectors are inexpensive, passive, long-lived

- Sensitive receivers, internal gain

- Wideband receiving system

- Stable calibration in range and angle

- Possible photographic record vs. stars

FIGURE 1

RETROREFLECTORS IN SPACE

EARTH SATELLITES

Date	Satellite	Agency
Oct 1964	BE-B	GSFC
Apr 1965	BE-C	GSFC
Nov 1965	GEOS-I	GSFC
Feb 1967	DI-C	French
Feb 1967	DI-D	French
Jan 1968	GEOS-II	GSFC
Dec 1970	PEOLE	French

LUNAR REFLECTORS

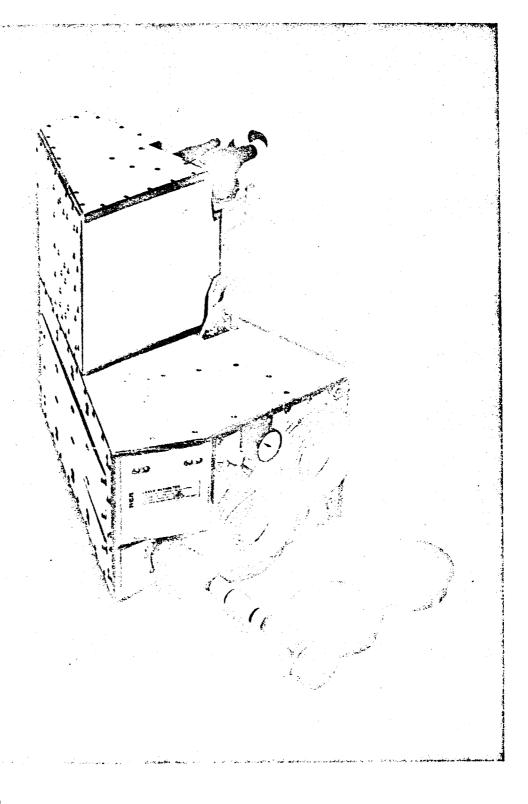| Mission	Country
Apollo 11	USA
Apollo 14	USA
Lunachod	USSR
Apollo 15	USA

FIGURE 2

FIGURE 3

We shall review the principles and performance experience of the
laser satellite ranging systems developed and operated at GSFC and
then extrapolate them to possible space-borne altimetry systems.
We shall not describe a definitive design, but merely present a
representative list of parameters which may serve as a basis for
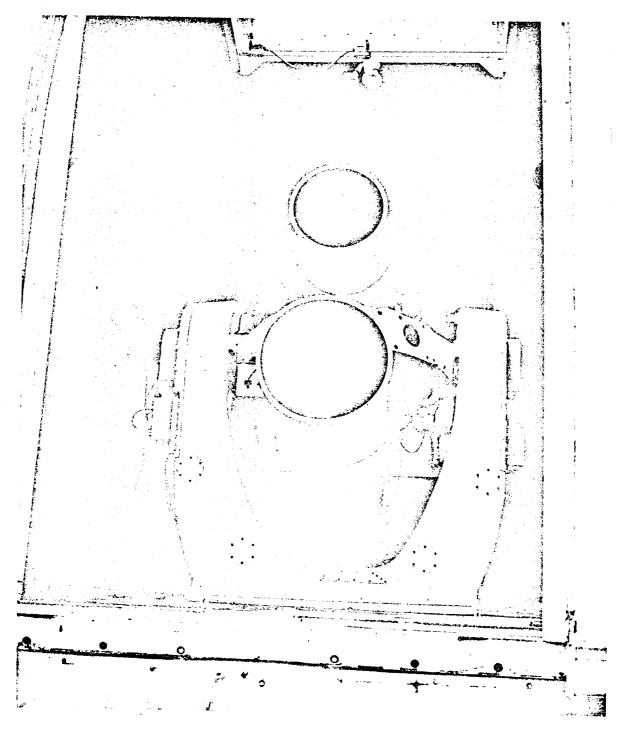discussing alternative approaches.

Laser Satellite Ranging Systems

The retroreflector array on BE-B and BE-C is shown in Figure 4.
Each reflector is made of fuzed silica in the shape of a cube corner
with a silvered coating on the three perpendicular reflecting faces.
The property of the cube corner reflector (see, e.g. Ref. 5, 6) is
that a ray entering the front face makes three reflections and
returns in the same direction from which it was incident. This
property is independent of the orientation of the cube corner except
that the effective area of the entrance aperture will decrease
rapidly as the angle between the incident ray and the symmetry axis
increases. The Beacon-Explorer Satellites were oriented along the
earth's magnetic field, and could spin about that direction. In
order to insure that a sufficient number of reflectors would have a
favorable aspect with respect to a ground station (in the northern
hemisphere), the reflectors were arrayed over a truncated pyramid
on the north-seeking end of the satellite. A similar arrangement
was necessary on the French Diamont Satellites, which were also
magnetically oriented. On the other hand, the GEOS Satellites are
oriented by the earth's gravity-gradient, and so one face always
points down. On these, the laser reflectors are arranged in a plane
on the face directed to the earth.

The arrangement of the reflectors is significant here, because not
only does it determine how the reflected signal intensity will vary
over a satellite pass, but it also determines, indirectly, the
precision with which we will be able to measure range. A sharp
pulse incident on the satellite will be reflected as a pulse spread
over the various distances to each of the individual reflectors.
Since BE-B and BE-C are .5 meters in diameter and GEOS-I and II are
1 meter in diameter, typical signal pulse widths due to reflector
array geometry correspond to range uncertainties between 20 and
50 cm.

Figure 5 is a picture of the experimental laser satellite tracking
station at the Goddard Space Flight Center. It uses an altitude-
azimuth mount adapted from a surplus Nike-Ajax radar. Five optical
telescopes are seen on the central elevation ring, but only two are
actually used for the laser ranging function. The small telescope
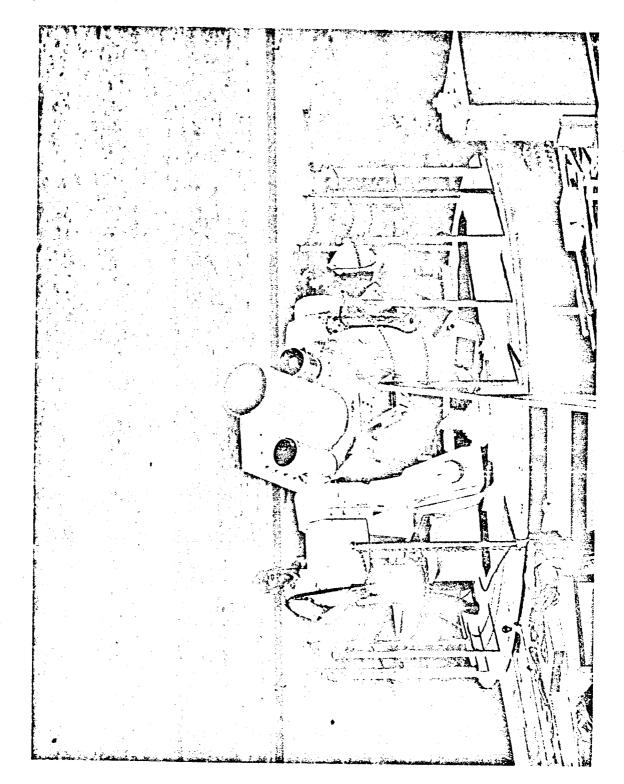
FIGURE 4

NASA G-71- 965

FIGURE 5

at the left end of the elevation axis is a low power telescope used for rough setting during boresighting. Above the ring, on the left is the laser collimating telescope (5" aperture); top center is the reflecting telescope (16" aperture) normally used as receiver in the ranging system; top right is a high power telescope used occasionally by an operator to provide manual correction to the pointing of the system if the satellite target is visible; bottom center is a reflecting telescope (20" aperture) used experimentally during NASA's program to improve the techniques of laser tracking; bottom right is a star tracker used sometimes to lock the system onto a bright object for alignment.

A mobile laser tracking system developed and operated by GSFC is shown in Figure 6. It differs from the fixed station described above in that the laser itself is not mounted on the moving telescope platform, but is placed below the platform. The laser beam is reflected from five plane mirrors and moves through the moving axis before finally passing through the collimating telescope shown on the left side of the elevation platform. This has the advantage that cooling fluid hoses and power cables need not be made flexible to move during a satellite pass, and the laser can operate in a fixed position. The disadvantage is that we suffer losses during the additional reflections. The central telescope (16" aperture) is the receiving antenna, and the telescope at the right is used by an operator, as shown, to help aim the system when the target is visible. The electronics and control system is housed in an instrumentation van and the opto-mechanical system is carried on a trailer bed when being moved.

Operation of the system is controlled by a central computer, Figure 7. From the elements of the expected orbit, the computer generates the angle coordinates which are used to operate the mount servo control system. The laser is fired once per second, the beam passing through the collimating optics, which supplies the required antenna gain. The transmitter power is sampled and recorded, and used to start the "range time interval unit". When the echo pulse is received its intensity is also recorded and it is used to stop the range counter, which has a resolution of 0.1 nanosecond. The receiving detector is gated "on" only for a short interval at a time predicted by the central computer, so as to minimize the possibility that the range counter would be stopped by a noise pulse. The block diagram also shows an ability to generate angle tracking corrections, which is now being installed. Finally, for each pulse, we record time of the measurement, time of flight, energy of the transmitted and received pulses, and the aximuth and elevation angles.
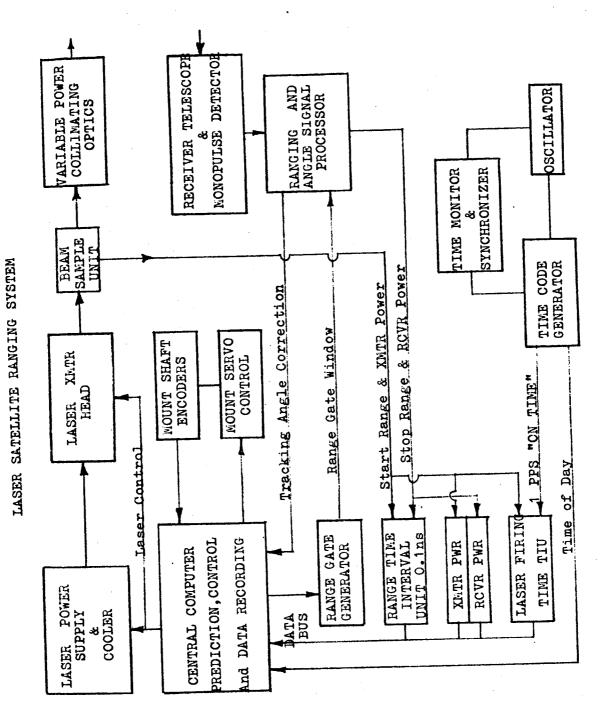
FIGURE 6

LASER SATELLITE RANGING SYSTEM

FIGURE 7

8-10

In order to appreciate the problems associated with design of a laser altimeter, it may be instructive to review the parameters of the satellite tracking system. Referring to Figure 8, we consider a laser pulse of E_T joules from a ruby laser radiating red light with a wavelength λ of 6943 Angstroms. Ruby lasers are normally not diffraction limited, but radiate into a solid angle determined, in part, by strains in the crystal. The transmitting telescope diminishes the divergence cone to an angle θ_T, which we choose to be compatible with our ability to point confidently to a rapidly moving satellite. The energy which strikes each reflector, of diameter a, at a distance R, is therefore

$$\frac{E_T \alpha}{\Pi/4 \; \theta_T^2} \cdot \frac{\Pi/4 \; a}{R^2} \qquad \text{joules} \qquad (1)$$

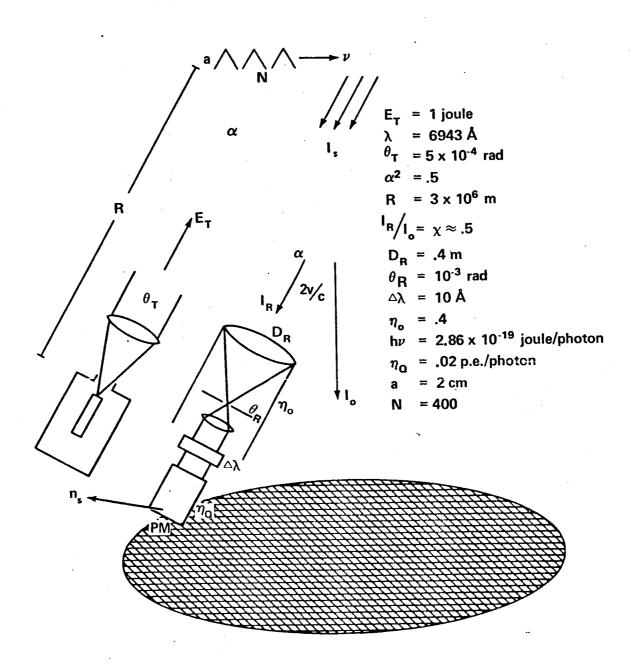where α is the transmission of the atmosphere.

The pattern of the reflected light should be similar to that of radiation through a circular aperture of radius a (even though the entrance aperture is hexagonal rather than circular). The intensity at the center of the pattern (Reference 7), when the total energy is E, is given by

$$I_o = \frac{E \cdot \Pi/4 a^2}{\lambda^2} \qquad \text{joule/steradian} \qquad (2)$$

As illustrated in Figure 8, the reflected spot will not be centered around the transmitter, as might be expected from the retro-reflective properties of the cube corner, but will be shifted in the direction of the satellite's velocity v by an angle 2 v/c. Since the receiver and transmitter are mounted together, the receiver will see an intensity reduced by a fraction x of the central intensity. The reflected energy thus collected by the telescope, of diameter D_R is

$$\frac{\Pi E_T \alpha^2 a^4}{4 \; \theta_T^2 \; R^2 \; \lambda^2} \cdot \frac{\Pi/4 \; D_R^2}{R^2} \cdot x \qquad \text{joule} \qquad (3)$$

8-11

E_T = 1 joule

λ = 6943 Å

θ_T = 5×10^{-4} rad

α^2 = .5

R = 3×10^6 m

I_R/I_o = $\chi \approx .5$

D_R = .4 m

θ_R = 10^{-3} rad

$\triangle\lambda$ = 10 Å

η_o = .4

$h\nu$ = 2.86×10^{-19} joule/photon

η_Q = .02 p.e./photon

a = 2 cm

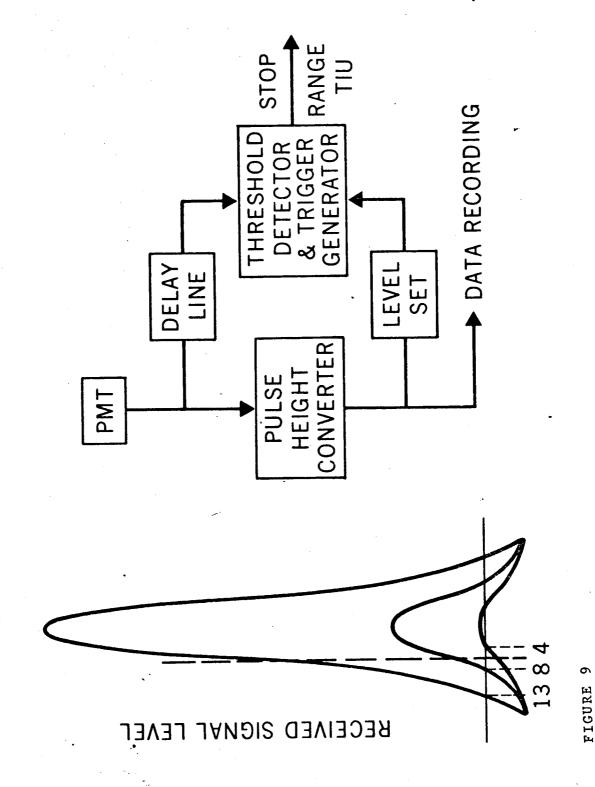N = 400

SATELLITE RANGING PARAMETERS

FIGURE 8

The energy received is focused, with optical efficiency η_o, through a filter with passband $\Delta\lambda$, onto a photomultiplier which converts photons into photoelectrons with a quantum efficiency η_Q. Converting the energy given by (3) into photons with energy $h\nu$, and multiplying by the number of satellite reflectors N, the number of signal photoelectrons becomes
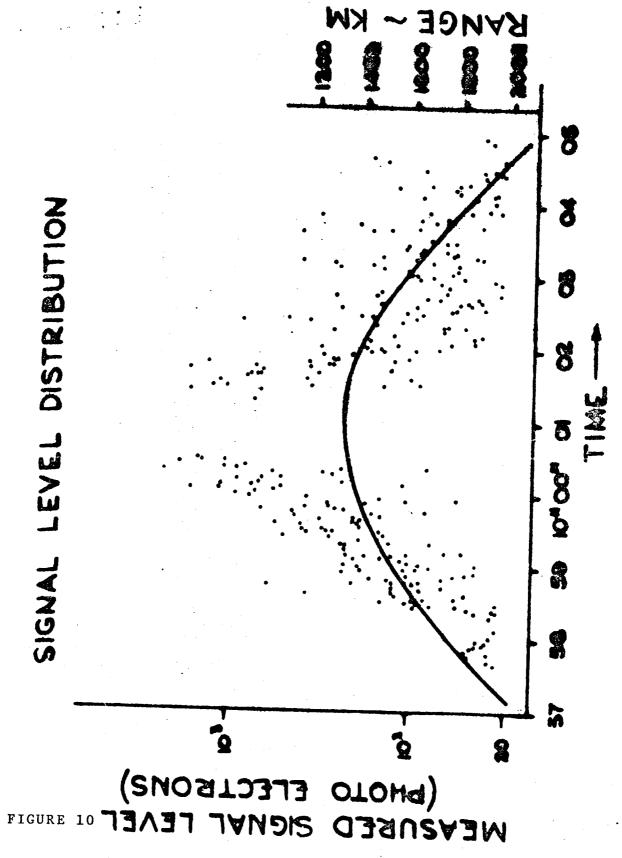
$$n_s = N\frac{\Pi^2 E_T \alpha^2 a^4 D_R{}^2 x\eta_o}{16\ \theta_T{}^2 R^4 \lambda^2} \cdot \frac{\eta_Q}{h\nu} \qquad (4)$$

Using the hypothetical values for the parameters that are listed in Figure 8, we arrive at a signal of 2000 photoelectrons. This is actually a very good signal. Normally, a signal of 20 photoelectrons is set as the detection threshold. Noise pulses produced by daylight sky background radiation within the milliradian receiver field of view which passes through the wavelength filter very rarely result in false alarms at this threshold level.

If we grant, then, that signals are strong enough to permit confident detection, how shall we use them to measure range in the most precise and accurate manner? Typical ruby laser pulse widths used so far for satellite ranging are 15 nanoseconds (at half-intensity). This would correspond to over 2 meters of range uncertainty. In the ocean surface altimeter, even though we expect to use much shorter laser pulses, the ocean wave structure would introduce similar pulse spreading. How can we achieve 10 cm accuracy?

In Figure 9, we see that a constant threshold level, set to trigger a counter when the leading edge of a received pulse reaches a pre-fixed value, will result in a measured time which depends upon the height of the received pulse. The larger the pulse, the earlier the trigger will be activated, with respect to the center of the pulse. On the other hand, the figure also shows that, with approximately Gaussian shaped pulses, the half-maximum intensity seems always to occur at the same time. The technique which is now used is to trigger the counter when the pulse reaches half the maximum intensity, in accordance with the block diagram shown. Such an arrangement is necessary because the energy of received signal pulses will vary over orders of magnitude through the course of a satellite pass. Figure 10 is the record of a typical pass. The general trend of signal level results from the inverse R^4 dependence, but the wide scatter in pulse height from shot to shot is due to variable aiming accuracy and

8-13

DYNAMIC THRESHOLD COMPENSATION

FIGURE 9

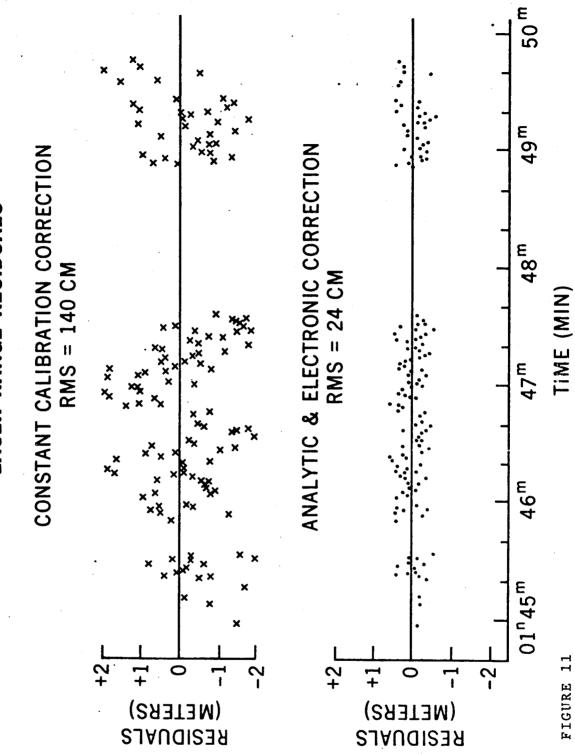SIGNAL LEVEL DISTRIBUTION

FIGURE 10

8-15

scintillation in the intensity of the reflection back to a given spot on the ground. Superposition of reflections from all of the cube-corners in the satellite array gives rise to a random inter-ference pattern with sharp contrast between bright and dark spots.

If a constant trigger level were used to stop the range counter, we could expect a wide variation in measured satellite range. This is illustrated in Figure 11. All of the ranges measured during a single pass are fitted to an orbit. That is, the parameters for an orbit, consistent with the latest SAO model of the earth's gravitational field, are adjusted to yield a least-square fit to the observed ranges from the known ground station. The individual residual difference between each measured range and that calculated from the best-fit orbit is then plotted as shown. The upper curve shows range residuals when a constant trigger threshold level is used, resulting in an rms deviation of 1.4 meters as a measure of scatter. In the lower curve, we have stopped the counter at the half-max time and also applied an analytic calibration correction. The range scatter has been reduced to 24 cm. This technique is now standard in all GSFC laser satellite tracking.

It is interesting to note that the accuracy of laser tracking (i.e., ability to calibrate instrumental delays and to prevent drift) is also commensurate with the precision (or scatter), which is now between 20 and 50 cm on individual short arcs. This has begun to uncover new effects which will probably require refinements in our description of the gravitational field. An example is shown in Figure 12. Recently, BE-C was tracked simultaneously over a period of several months, by two laser stations: the fixed one at Goddard (GODLAS) and the Mobile one in upper New York State at the Seneca Army Depot (SENLAS). If range measurements from any one pass were fit to an orbit, the residuals of individual points would look like those in Figure 11. The orbit parameters could be adjusted well enough so that over a short arc no systematic trend could be noticed in the residuals. However, in Figure 12, the orbit parameters have been adjusted to fit four successive passes from one of the stations. The orbit was made consistent with the latest SAO gravitational model. Yet, even the best fit was not able to remove the obvious short term fluctuation in the residuals. Similar patterns are observed from the second station.

Although the systematic fluctuations from the best-fit four-pass orbit exceed ± 5 meters, the scatter of measurements about the smooth sinu-sodial curve is on the order of 20 cm rms. Similar results were ob-tained during all opportunities to track four successive orbits from

LASER RANGE RESIDUALS

FIGURE 11

Four Consecutive and Simultaneous Laser Passes from BE-C

Godlas

Range
Resid-
uals
in
Meters

Senlas

best orbit

+5

0

-5

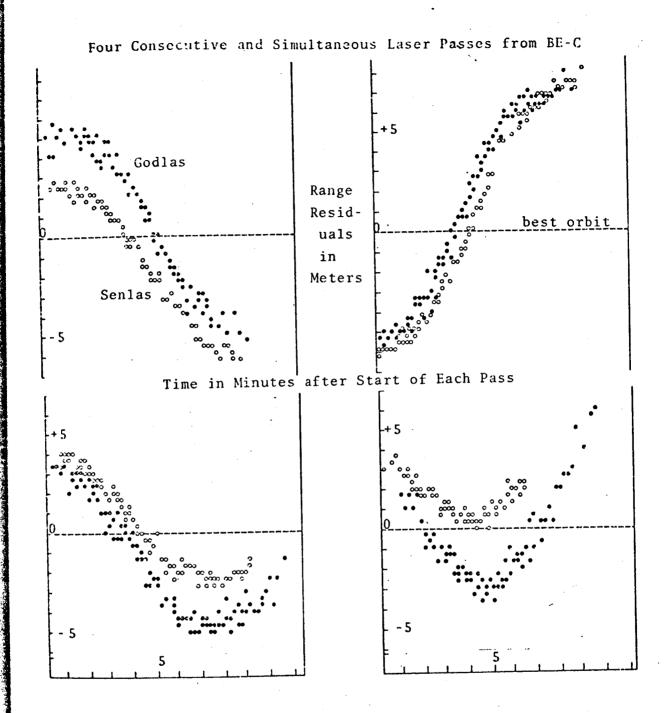Time in Minutes after Start of Each Pass

+5

0

-5

5

+5

0

-5

5

FIGURE 12

the same station. Although it is not clear which geopotential terms must be corrected to account for this residual pattern, the period of the effect suggests deficiencies in low degree and order terms in the gravity field.
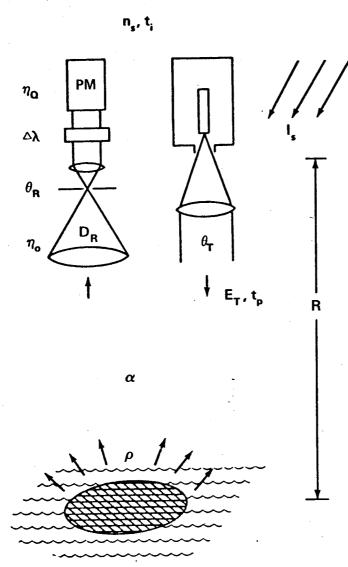
Laser Altimeter Design

We will discuss the simple-minded concept sketched in Figure 13, as an introduction to the significant factors for a space-borne laser altimeter. A neodymium-YAG laser was chosen, with frequency doubling, so that the wavelength of the transmitted radiation is 5300 Angstroms. This seems a reasonable choice, because of the sensitivity of state-of-the-art detectors for green light. Trade-off studies in this and other areas must be performed before choosing a final design. Pulse energy E_T of 0.25 joule and pulse width t_p of 3 nsec implies a Q-switched, but not necessarily mode-locked laser.

The laser collimating antenna will produce a divergence cone with diameter (θ_T) radians, and the spot of illumination on the ocean (footprint) will have a diameter $\theta_T R$. The numerical values we have chosen give rise to a 100 meter circle, which may be awkward because it is close to the length of a typical gravitational wave. However, this parameter is not at all critical, and can be greatly expanded or contracted. It should be noted, however, that 0.25 joules spread over a 100 meter circle produces an intensity of 3.2×10^{-11} joule/mm^2 on the surface, which is far below the danger threshold of 1.25×10^{-7} joule/mm^2 (U.S. Army).

For the reflectivity, ρ, of ocean water, we take the value 2% derived from the Fresnel formula for normal incidence, using an index of refraction of 1.33. Further, we assume that the angular distribution of reflected radiation is that which corresponds to a diffuse reflector. If there is any specularity to the reflection at vertical incidence, then the signal strength will be much greater than the estimate given here. This is a parameter that will probably depend very critically upon "sea state", and should be studied as a preliminary to final system design. We should also expect a good deal of scintillation, similar to that now observed from satellites. For diffuse reflection, then, the intensity reflected vertically up is

$$\frac{E_T \rho \alpha}{\Pi} \qquad \text{joule/steradian} \qquad (5).$$

8-19

$$E_T = 0.25 \, j$$
$$\lambda = 0.53 \, \mu m \qquad R = 10^6 \, m$$
$$t_p = 3 \, nsec \qquad \alpha^2 = 0.5$$
$$\theta_t = 10^{-4} \, rad$$

$$\rho = 0.02$$
$$D_R = 0.3 \, m$$
$$\theta_R = 1.5 \times 10^{-4} \, rad$$
$$\triangle\lambda = 10 \, \text{Å}$$
$$\eta_o = 0.4$$
$$\eta_Q = 0.2 \, p.e./photon$$
$$t_i = 20 \, nsec$$
$$h\nu = 3.75 \times 10^{-19} \, j/photon$$
$$I_s = 0.1842 \, w/cm^2 - \mu m$$

ALTIMETER PARAMETERS

FIGURE 13

The receiving telescope has a field of view θ_R which is large enough to see the entire illuminated spot. It collects the energy

$$\frac{E_T \rho \alpha^2}{\Pi} \cdot \frac{\Pi/4 \; D_R^2}{R^2} \qquad \text{joule} \qquad (6)$$

After passing through the optical system, whose efficiency is η_o, the photons are converted by the detector into n_s photoelectrons, with quantum efficiency η_Q:

$$n_s = \frac{E_T \rho \alpha^2 D_R^2}{4 \; R^2} \cdot \eta_o \cdot \frac{\eta_Q}{h\nu} \qquad (7)$$

Using the values listed in Figure 13, we arrive at an average signal of 12 photoelectrons per transmitted pulse.

Competing with this, we have various noise sources. We only consider two which appeared most likely to be significant: sunlight and signal fluctuation. Sunlight illuminating the ocean surface within the receiver field of view and within the optical filter passband is given by

$$I_s \Delta\lambda \cdot \frac{\Pi}{4} \; \theta_R^2 R^2 \alpha \qquad \text{watt} \qquad (8)$$

where I_s (Figure 13) is found in Reference 8.

In order to discriminate against noise sources, Figure 14 shows a post-detection filter and threshold detector. The filter is essentially an integrating circuit which stores the charge received over an interval t_i, and t_i is set to represent the longest pulse we may expect to receive. Assume that t_i is set to 20 nanoseconds, since that is the pulse spreading due to reflection from waves 3 meters high. Then, the threshold detector will determine whether the energy received during any 20 nanosecond interval should be considered a valid signal. The sunlight given by equation (8) which falls within t_i, is then the significant solar background. This is reflected

(diffusely), collected by the receiving telescope, and converted into noise photoelectrons:

$$n_s = I_s t_i \Delta\lambda \cdot \frac{\Pi}{4} \theta_R^2 R^2 \alpha \cdot \frac{\rho\alpha}{\Pi} \cdot \frac{\Pi/4 \ D_R^2}{R^2} \cdot \eta \cdot \frac{\eta_o}{h\nu}$$

$$= \frac{\Pi I_s t_i \Delta\lambda \theta_R^2 \rho\alpha^2 D_R^2 \eta_o \eta_o}{16 \ h\nu} \qquad (9)$$

Substituting the numerical parameters from Figure 13 tells us that .04 photoelectrons are collected from reflected sunlight during the integration period t_i. This is clearly not a significant noise background when compared to an expected signal of 12 photoelectrons. (The background computed here is equivalent to 2×10^6 noise photoelectrons per second, which is generally equivalent to the sky background now observed in satellite tracking.)

The second type of noise which we must consider is that arising from fluctuations in the number of signal photoelectrons arriving during each pulse. The statistics of discrete photoelectrons (Reference 9) tells us that if we expect n_s photoelectrons within a measuring interval, the root-mean-square deviation from the average will be $\Delta n_s = \sqrt{n_s}$. Thus, in our case, the ratio of signal-to-rms fluctuations will be

$$\frac{n_s}{\Delta n_s} = \sqrt{n_s} = \sqrt{12} = 3.5 \qquad (10)$$

Such a poor signal-to-noise ratio can have a profound effect in limiting the range measuring precision.

This can be illustrated by considering the block diagram of Figure 14 (taken from Reference 1). In this system, after determining that a pulse is a true laser reflection by satisfying the threshold criterion, the gate is opened and the pulse is sent to an integrator. When the integral is equal to half the total area under the pulse curve, a signal is generated to stop the range gate. Thus, the centroid of the pulse is used for measuring range. This may be the most valid measure for mean sea level when the pulse is spread by
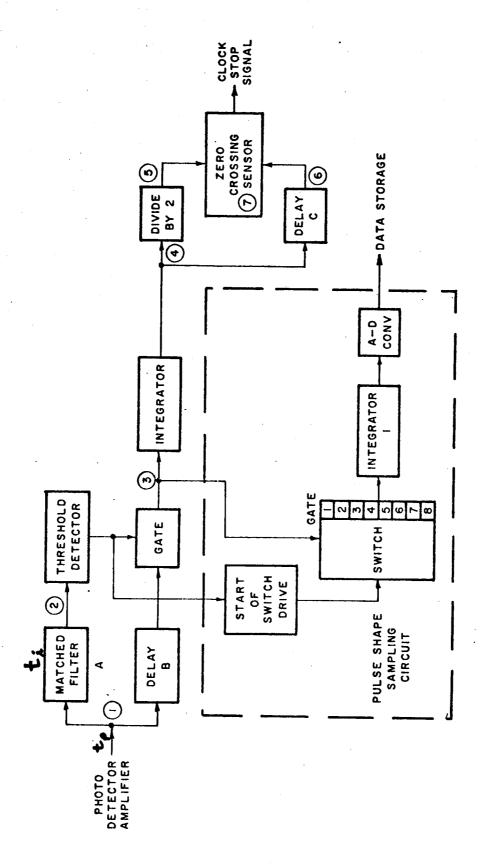
FIGURE 14

wave height. Any other point in the pulse may be used, if suggested
by a detailed study of ocean wave shapes.

If, however, the random arrival of pulses serves to distort the
shape of the pulse, then the measured centroid position will not be
a true measure of mean sea level. It can be shown that the fractional
error in finding the centroid is given by the ratio of noise to signal.
If the pulse were 20 nanoseconds long, corresponding to 3 meter waves,
and S/N = 3.5, we could expect an rms error of 85 cm in finding mean
sea level. If waves were 2 meters high, and we wanted a precision of
10 cm, we would need $\sqrt{n_s}$ = 20, or n_s = 400.

Figure 14 also illustrates one technique for studying the shape of the
pulse, and thereby inferring ocean wave structure. By dividing the
pulse into a number of time-slot channels, each 2 or 3 nanoseconds
wide, we can measure the number of photoelectrons in each channel and
read them out sequentially.

An additional obvious source of error arises when the rays are not
vertical. If we limit the error from this source to 10 cm, then
the rays must not deviate by more than 1.5 minutes of arc. This
would be satisfied by a divergence cone of 1 miliradian, producing
a footprint 1 kilometer in diameter.

The assumptions upon which this paper is based may be quite conser-
vative (especially that of diffuse reflection from the ocean surface).
It appears that the present state-of-the-art would make a space-borne
laser altimeter practical within a reasonable development cost.
Whether or not such a task is undertaken must depend upon its expected
value to oceanography and geodesy. It cannot operate through cloud
cover, which probably limits it to no more than 50% of the ocean area
at a given time. On the other hand, its superior precision and
accuracy may justify a laser altimeter as a supplement to a microwave
altimeter. While the latter can provide continuous coverage, the
former will provide accurate calibration checks and permit possible
study of detailed fine structure. The laser could, in addition,
measure height above lakes and above small inexpensive retroreflectors
placed at critical spots around the globe.

Apollo 15 Laser Altimeter

Information about the Apollo 15 Laser Altimeter was obtained in very brief telephone conversations with Mr. J. H. Woodward and Mr. R. C. Guyer, RCA, Aerospace Systems Division, Burlington, Massachusetts. It is presented here to the best of the author's memory and therefore should not be considered reliable.

The altimeter (built by RCA) operated in conjunction with a metric camera (built by Fairchild) taking mapping photos of the lunar surface from the Command and Service Module as it orbited the moon waiting for Ascent Stage to return. Altimeter and camera were boresighted so that a precise range could be found for a well-defined spot on the photograph. From this, one could convert angular distances on the photo into accurate linear distances on the lunar surface.

The altimeter operated continuously for 24 hours at the moon, performing up to specifications. Then several malfunctions occurred which terminated the operation. Apparently, there was a high voltage breakdown in a "safety circuit". There also seemed to be severe contamination of the telescope optics, perhaps because of proximity to a discharge port for waste fluid. RCA engineers believe they can correct the deficiencies and that the malfunctions did not reflect inherent weaknesses in the system itself. It is expected to fly again on Apollo 16 and Apollo 17.

The altimeter operated between altitudes of 40 mi and 80 mi, and had a fixed detector gate corresponding to this range of delays. The laser was a Q-switched ruby laser, operating once every 16 seconds. Transmitter divergence was 300 microradians, receiver field of view was 200 microradians. The receiver was a 16 power reflecting telescope with 4-inch diameter aperture. The range measuring circuitry was built around a 150 MHz counter and had a precision of ± 1 meter. The package was an irregular shape with a volume of about 1 ft ^{3} and weight of 50 lb. It consumed about 50 watts when operating. The observed signal strengths implied that the lunar surface had reflectivity between 7 and 18%.

That the Lunar Laser Altimeter is a simpler problem than that presented by an ocean surface altimeter from earth orbit, can be seen by a rapid calculation. Using the formula already developed for the number of signal photoelectrons from a diffuse reflecting surface,

$$n_s = \frac{E_T \rho \alpha^2 D_R^2 \eta_o \eta_Q}{4 \, R^2 \, h\nu}$$

We use the following values:

E_T = 0.25 joules $\qquad\qquad$ η_o = 0.4

ρ = 0.1 $\qquad\qquad\qquad$ η_Q = .02 p.e./photon

α^2 = 1 $\qquad\qquad\qquad$ R = 100 km

D_R = 0.1 meter $\qquad\qquad$ $h\nu$ = 2.857 x 10^{-19} joule/photon

This results in a signal of 175 photoelectrons per pulse, which is quite comfortable, under the circumstances.

REFERENCES

1. "Space Geodesy Altimetry Study", Raytheon Company, NASA Contract Report, NASA CR-1298, March 1969

2. "Optical Altimeter Receiver Systems Study and Design for a Spaceborne Laser Altimeter", ADCOM Final Report for Contract Number NAS 12-2058, May 31, 1969

3. "Development and Fabrication of a Laser Tracking Receiver System", ADCOM Final Report for Contract NAS 12-2184, October 1970

4. Private communication with Jason Woodward, RCA Corporation, Bulington, Massachusetts

5. P. R. Yoder, Jour. Optical Society of America $\underline{48}$ No. 7, p. 496 (July 1958)

6. R. F. Chang, et al, Jour. Optical Society of America $\underline{61}$, 431, (April 1971)

7. Born and Wolf, Principles of Optics, Pergamon Press, 1959, Page 394

8. "Solar Electromagnetic Radiation", NASA Document No. NASA SP-8005, Space Vehicle Design Criteria (Environment), Revised May 1971

9. "Laser Receivers", M. Ross, John Wiley & Sons, New York, 1966, p. 32

E